Advances in Nano Research, *Vol. 11, No. 5 (2021) 453-466*
https://doi.org/10.12989/anr.2021.11.5.453

Ultra-robust bonding between MXene nanosheets and stretchable, self-healable microfibers

Yoo Bin Shin[1], Youngmin Kim[2], Chang Goo Kang[3], Jung-Min Oh[1] and Jong-Woong Kim*[1]

[1]*School of Advanced Materials Engineering, Jeonbuk National University, 567 Baekje-daero, Deokjin-gu, Jeonju 54896, Republic of Korea*
[2]*Display Research Center, Korea Electronics Technology Institute, 68 Yatap-dong, Bundang-gu, Seongnam 13509, Republic of Korea*
[3]*Advanced Radiation Technology Institute, Korea Atomic Energy Research Institute, 29 Geumgu-gil, Jeongeup-Si, Jeollabuk-Do 56212, Republic of Korea*

(*Received July 19, 2021, Revised August 20, 2021, Accepted August 22, 2021*)

Abstract. To develop a reliable fibrous device, a strong bond between conducting materials and fibers must be ensured. While the external surface of the film is relatively flat, making it easy to deposit the electrode materials uniformly, the walls of the polymer fibers inside the porous film pose a greater challenge for ensuring a uniform coating and robust bonding with electrode material. Herein, a microfibril-based porous film was prepared by electrospinning polybutadiene-based urethane (PBU), a newly synthesized self-healing polymer, and Ti_3C_2-based MXene nanosheets were coated thereon to fabricate a pressure sensor whose resistance decreases with pressure. The PBU microfibrils were crosslinked under mild conditions via Diels-Alder (DA) reaction by exploiting low activation energy of the PBU. An exceptionally robust bonding between the PBU and MXene was enabled by subjecting the PBU to a retro-DA and subsequent DA reactions. The temporary increase in surface fluidity of the PBU leaded to a conformal contact between the MXene and fibers without collapse of fibrous structure, resulting in an ultra-robust bond between them. A stretchable and self-healable pressure sensor was implemented by removing unnecessary MXenes by applying ultrasonic energy to the thus-fabricated sample. The fabricated sensor showed a pressure sensitivity of around 27.9 /kPa for a wide range of pressure which is the highest level among the reported stretchable self-healing pressure sensors, while maintaining its performance even after 1000 cycles of stretching and pressing. Further, sensors attached around the carotid artery could be used to precisely detect P-, T-, and D-waves arising from blood pressure.
Keywords: MXene; polybutadiene; pressure sensor; Ti_3C_2Tx; urethane

1. Introduction

The recent development of epidermal electronic devices enables close tracking of physiological signals and physical activities of the human body without deteriorating the quality of life. Pressure sensors are regarded as one of the key components of epidermal electronics. Considerable efforts are being devoted to the development of highly sensitive pressure sensors that are capable of detecting physical stresses in real time (Zhu *et al.* 2018, Lee *et al.* 2020a, Ruth *et al.* 2020, Xiong *et al.* 2020, Bai *et al.* 2020, Wang *et al.* 2020, Huang *et al.* 2020, Yu *et al.* 2020, Yu et al. 2019, Zeng et al. 2020). Pressure sensors must fulfill the requirements of high sensitivity, mechanical stretchability for imperceptible wearability, long-term reliability, and low-cost fabrication for practical application in epidermal electronics (Zhu *et al.* 2018, Lee *et al.* 2020a, Ruth *et al.* 2020, Xiong *et al.* 2020, Bai *et al.* 2020, Wang *et al.* 2020). Moreover, given that such pressure sensor will be subject to continuous tactile contact and repeated cycles of pressure application by external objects, ability to recover from ruptures and physical damages, which are likely to be caused by repeated application of stresses (Mehrez *et al.* 2020), would be a desirable quality for the sensors. Since the introduction of pressure sensors with pyramidal structures by Mannsfeld *et al.* (2010) many similar structures have been proposed for pressure sensors, which have resulted in significantly enhanced sensitivities compared to those of solid film-based sensors (Shi *et al.* 2018, Li *et al.* 2018, Yang *et al.* 2019, Sang *et al.* 2019, Xiao *et al.* 2018). This enhancement in sensitivity is owing to the presence of vacant regions in the sensors, which greatly increase the deformation of the material constituting the sensor when subjected to pressure, and consequently, increase the stress applied to the electrode. However, the fabrication of such structures requires highly complex and costly procedures, often involving semiconductor processing, which poses major obstacles to mass production. Similar concepts with less complicated processes have been also previously reported, but they suffered from relatively low pressure sensitivity (Huang *et al.* 2020, Yu *et al.* 2020, Yu et al. 2019, Zeng et al. 2020). These roadblocks can be overcome by electrospinning, a relatively simple process that is capable of producing films having porosities similar to those of sensors implemented by semiconductor fabrication processes (Kalani *et al.* 2020, Zhu *et al.* 2020). There are multiple reports of porous films made from fibrous polymers obtained by electrospinning (Li *et al.* 2021, Moraveji *et al.* 2021, Liu *et al.* 2018).

The following requirements must be satisfied to produce

*Corresponding author, Professor,
E-mail: wyjd@jbnu.ac.kr

ISSN: 2287-237X (Print), 2287-2388 (Online)

stretchable and self-healable pressure sensors with high sensitivity by the electrospinning. First, the polymer to be employed in the electrospinning should be highly elastic and self-healable. Second, the self-healing process should not result in a collapse of the network structure. Finally and most importantly, the electrospun fibers should be capable of robust bonding with the electrode materials participating in the functioning of the sensor. In general, polymers such as polycarbonate (Baby *et al.* 2019), polybenzimidazole (Zholobko *et al.* 2020), polyacrylonitrile (Wang *et al.* 2019), polycaprolactone (Moraveji *et al.* 2021), and polylactic acid (Huang *et al.* 2018) have been used in electrospinning. However, they exhibit low elasticity and high strength, making them unsuitable for stretchable porous films. Although polymers that form hydrogen bonds are potential candidates for producing self-healing films, they are unsuitable for electrospinning owing to their low strength and surface stickiness. In addition, polymers capable of undergoing the Diels-Alder (DA) reaction usually have high cross-linking temperatures, which could result in coalescence between adjacent fibers during curing or healing. Coalescence between electrospun fibers may occur owing to excessive thermal expansion and increased flowability of the polymers at high temperatures. Furthermore, the process necessary for the self-healing should not cause a significant increase in polymer flowability to ensure that the porous network structure does not collapse during the self-healing process. For DA reaction-based polymers, self-healing is implemented by the reversal of crosslinking by retro-DA reactions, followed by re-establishment of the crosslinks by a DA reaction. Therefore, if retro-DA and subsequent DA reactions occur at a mild condition, the self-healing process will not lead to a collapse of the fibrous network structure of the film.

Satisfying the last condition is most challenging, as the morphology of the porous film, where the electrode material must be deposited, varies with location. While the external surface of the film is relatively flat, making it easy to deposit the electrode materials uniformly, the walls of the polymer fibers inside the porous film pose a greater challenge for ensuring the deposition of a uniform coating of the electrode material such that it is securely immobilized on the surface. Since the fiber-based pressure sensor is operated by repeated physical contact and shearing between electrode materials on the fiber surface, bond stability between the electrodes and fibers is very important in terms of the stability of measurement signals and the long-term reliability. Unfortunately, however, most of the studies so far have been limited to the improvement of wettability and short-term adhesion simply through the surface treatment of fibers (Luo *et al.* 2021, Fu *et al.* 2021, Cheng *et al.* 2021). In that case, it should be noted that there is a limit to the effect of surface treatment inside the film when the porosity is very low.

We report the fabrication of a highly sensitive pressure sensor with mechanical stretchability and self-healing ability using electrospinning. We synthesized a novel polybutadiene-based urethane (PBU) for use in electrospinning to create a microfibril-based porous film. The PBU is highly elastic and forms DA adducts at a low temperature. The low-temperature DA reaction enabled crosslinking between the electrospun microfibrils, which improved the mechanical stability of the film and conferred self-healing ability to the film, without causing the collapse of the porous networked structure. In order to use the porous PBU film as a pressure sensor, we coated Ti_3C_2-based MXene electrodes on its surface and inner walls. Ti_3C_2 MXene-based electrodes have attracted great attention due to their hydrophilic surfaces and high metallic conductivities, which have enabled promising performance in sensors and capacitors (Zeng *et al.* 2021, Cai *et al.* 2019, Chen *et al.* 2019). Thereafter, we induced a retro-DA reaction followed by a DA reaction in the polymer microfibril surfaces at low temperature to ensure that the MXene nanosheets formed secure bonds with the polymer surfaces, without causing a collapse of the porous network structure. This novel strategy brought about exceptionally strong adhesion between the MXene nanosheets and the polymer, resulting in a highly sensitive, stretchable and self-healing pressure sensor.

2. Experimental section

2.1 Materials

The polyol, HLBH-P 2000 was purchased from Cray Valley. Isophorone diisocyanate (IPDI), methyl ethyl ketone (MEK), glycerol 1,2-carbonate, furfurylamine, bis(3-ethyl-5-methyl-4-maleimidophenyl)methane (BMI), and ethyl-alcohol were purchased from TCI. Dibutyltin dilaurate, hydrochloric acid (HCl), hydrofluoric acid (HF), and lithium chloride (LiCl) were purchased from Sigma-Aldrich. A SYLGARD 184 elastomer kit was purchased from Dow Corning, USA. All chemicals were used as received without purification. Silver nanowires (AgNWs, average diameter = 21 nm, average length = 22 μm) dispersed in isopropyl alcohol (IPA) were purchased from Flexio, Korea. Ti (99.9%), Al (99.9%) and C powders were purchased from High Purity Materials, Japan.

2.2 Synthesis of polymers

HLBH-P 2000 (12.0 g, 6.0 mmol), diol **1** (1.29 g, 6.0 mmol), and IPDI (2.67 g, 12.0 mmol) were added to a flask containing MEK (15.0 g) and stirred till a clear solution was obtained. A catalytic amount of dibutyltin dilaurate was added to this solution. The mixture was stirred at 60 °C for 2 h, following which, a viscous solution of polybutadiene-based urethane (PBU **2**) was obtained. Diol **1** was synthesized as per the known method (Pyo *et al.* 2016). Polydimethylsiloxane (PDMS) was prepared by mixing the base and curing agent in the SYLGARD 184 elastomer kit in a weight ratio of 10:1.

2.3 Synthesis of Ti_3AlC_2 MAX precursor

Ti, Al and C powders taken in a molar ratio of 3:1.1:2 were suspended in ethanol by stirring at 350 rpm for 2 h. The powder mixture was then separated by vacuum

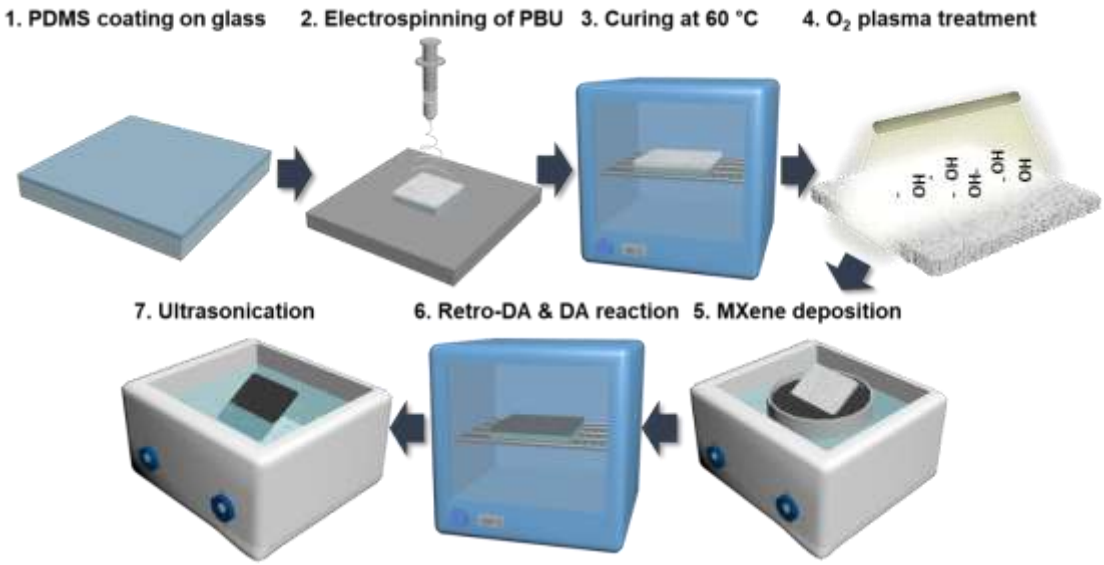

Fig. 1 Procedure for fabrication of stretchable, self-healing pressure sensors

filtration and dried in a vacuum oven at 70°C for 2 h. A vertical uniaxial press was used to compact the powder mixture at 25 MPa, after which the green compaction was charged in an alumina crucible and placed in the center of a Super-Kanthal furnace. The powder mixture was sintered at 1000°C for 1 h, and then at 1450°C for 3 h under argon. The flow rate of argon was maintained at of 2000 cc/min. The heating rate from room temperature to 1000°C was set to 10°C/min, while that from 1000°C to 1450°C was set to 5°C/min, in order to minimize the loss of Al, which has a melting point of about 660°C. The sintered powder was ground to a fine powder with a mean diameter of around 10 μm.

2.4 Fabrication of Ti_3C_2 MXene nanosheets

For synthesizing Ti_3C_2 MXene nanosheets from the Ti_3AlC_2 MAX precursors, the Al layer in the precursor was selectively etched using an HF-HCl mixed solution. First, 1 g of precursor powder was gradually added over the course of 1 min to 40 mL of etchant solution, prepared by mixing 24 mL of HCl (37 wt%), 6 mL of HF (49 wt%), and 12 mL of deionized water in a Teflon beaker. Then, the mixture was stirred at 35°C for 24 h using a Teflon magnetic stir bar. After the selective etching reaction, the acidic supernatant was decanted; the sediment then was washed with 40 mL of deionized water and separated by centrifugation at 5000 rpm for 5 min. The washing procedure was repeated until the pH of the supernatant reached a value of 6. Following this, the multilayer MXene sediment was separated from the deionized water by vacuum filtration. Subsequently, 2 g of LiCl (99.9%) was dissolved in 20 mL of deionized water and added to the multilayer MXene sediment for intercalation. This solution was shaken vigorously by hand for 10 min. Then, the solution was stirred at ambient temperature for 24 h and then washed repeatedly with 40 mL deionized water followed by centrifugation at 3500 rpm for 5 min to separate the MXene sediment, until a dark supernatant was obtained. The solution was centrifuged at 3500 rpm for 1 h, and the dilute green supernatant was decanted. The swollen sediment was re-dispersed in 40 mL of deionized water and centrifuged at 3500 rpm for 10 min to isolate the MXene supernatant from the sediment. The supernatant was then centrifuged at 10000 rpm for 20 min to separate the monolayer MXene sediment from deionized water. The obtained supernatant was discarded and the settled MXene slurry was recovered by vacuum filtration. The concentration of the MXene nanosheets in the MXene slurry was around 3 wt% (30 mg/ml). The slurry was diluted into a dispersion containing 0.8 wt% MXene by adding deionized water.

2.5 Fabrication of pressure sensor

The procedure for the fabrication of the stretchable, self-healing pressure sensor is depicted schematically in Fig. 1. First, to provide a hydrophobic surface for electrospinning, a PDMS layer was created on a cleaned glass substrate by spin-coating at 600 rpm for 30 s, followed by degassing in a vacuum desiccator for 30 min, and thermal curing at 120°C for 1 h. An electrospinning solution was prepared by adding BMI (1.32 g, 3.0 mmol) to the as-prepared PBU **2** solution (31 g), and stirred for 60 min. Without further purification, the solution was electrospun on the PDMS-coated glass substrate using a high-voltage electrospinning machine (ESR200R2, NanoNC, Korea) operated at 10 kV to obtain a microfibril-based porous film on the PDMS layer. The film was dried at room temperature for 10 min and cured at 60°C for 3 h inducing a DA reaction. The PBU porous film was peeled from the PDMS layer using a pair of tweezers. The film was subjected to O_2 plasma treatment in air for 10 min to create hydroxyl functional groups on the surface and inner walls of the PBU network. Then, the PBU porous film was dipped in the MXene nanosheet dispersion for 1 min, removed, and dried at room temperature for 30 min. To induce the retro-DA reaction, the sample was heat-treated at 120°C for 20 min. The sample was further treated at 60°C

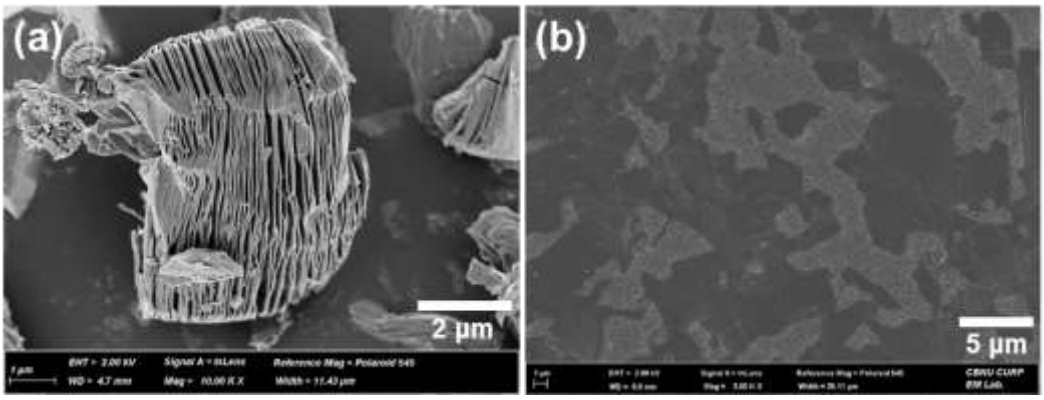

Fig. 2 FESEM micrographs of a multilayer Ti_3C_2 MXene and b individual Ti_3C_2 MXene nanosheets on a porous alumina plate

for 3 h to induce another DA reaction for solid adhesion between the MXene nanosheets and PBU porous film. The sample was then ultrasonicated for 10 min in an ultrasonic bath containing deionized water. Thereafter, the PBU porous film coated with MXene nanosheets was dried at room temperature for 60 min.

2.6 Characterization

^{1}H NMR spectra were recorded using an NMR spectrometer equipped with Bruker Top Spin 3.2 software (AscendTM 400, Bruker, Germany). Fourier transform infrared (FTIR) spectra were obtained in the wavelength range 600–4000 cm^{-1} in the attenuated total reflectance mode using an IRAffinity-1S FTIR spectrophotometer (Shimadzu, Japan). The glass transition temperature (T_g) of the PBU 2 was determined using a DSC-4000 calorimeter (PerkinElmer), and its molecular weight was measured by gel permeation chromatography (GPC) using an Agilent 1100 system (Agilent), respectively. Viscosity was measured using a digital viscometer (DV1MLVTJ0, AMETEK Brookfield, USA). The microstructure of the electrodes was investigated by field-emission scanning electron microscopy (FESEM), performed using a SUPRA40VP electron microscope (Carl Zeiss, Germany) equipped with an energy dispersive spectroscopy (EDS) detector. X-ray diffraction (XRD; XRD-6100, Shimadzu, Japan) was used for phase analysis, while the chemical composition of the MXene nanosheets was determined using X-ray photoelectron spectroscopy (XPS; ESCALAB 50, Thermo Scientific, USA). The sheet resistance (R_s) was measured using a non-contact measurement system (EC-80P, Napson Corp., Japan), while the resistance and current of the pressure sensor were measured using a source meter (Model 2461, Keithley, USA). The adhesion between the MXene and the PBU porous film was evaluated by applying and removing adhesive tape (Scotch Tape, 3M, USA). Mechanical stability, when subjected to repeated cycles of stretching, was investigated using an automatic stretch-testing machine (Jaeil Optical System, Korea). In the stretching test, tensile strains of up to 50% were used, and the samples were stretched at a rate of 10 cycles/min. Pressure sensing tests were conducted using a pushing tester (JIPT-120, Junil Tech, Korea). For determining each parameter, more than 10 samples were analyzed, and the average was reported as the value.

3. Results and discussion

The procedure for non-stop sintering at 1000°C and 1450°C for the synthesis of the Ti_3AlC_2 precursor was designed to yield a single phase of the precursor and ensure that no unreacted TiC remained as any TiC in the MAX powder contaminates the MXene nanosheets and degrades their bulk electrical properties (Seok *et al.* 2021). Further, the formation of TiO_2 was prevented by performing the sintering in an argon atmosphere. TiO_2 formed during the synthesis process has been reported to be primarily responsible for increasing the contact resistance between the MXene nanosheets (Lee *et al.* 2020b). The selective etching of the Al layer in the precursor MAX particles resulted in the formation of layered, accordion-like platelets comprising Ti_3C_2 MXene nanosheets as shown in Fig. 2(a). The selective etching of the Al layer is made possible by the fact that the bonding between Ti and C is stronger than that between Ti and Al. Fig. 3(a) shows the XRD patterns of the as-synthesized Ti_3AlC_2 MAX powder, Ti_3C_2 MXene powder acquired after the selective etching of Al, and individual MXene nanosheets. The XRD pattern of the MXene powder shows that it has a considerably lower degree of crystallinity and structural order than the MAX phase. The main peak corresponding to reflections from the (002) planes is broader than that in the pattern of the MAX phase, and shifted to a lower angle, 8.92° from 9.71° as a result of etching. This indicates a larger d-spacing (0.99 nm) between the layers in the MXene powder than in the precursor MAX, which originates from the removal of the Al layer from the MAX (Ti_3AlC_2) phase by etching, as reported elsewhere (Alhabeb *et al.* 2016). To obtain individually exfoliated MXene nanosheets, the stacked MXene platelets were intercalated by Li ions (from the LiCl solution) and subsequently delaminated. Figs. 3(b) (inset) and 2(b) shows FESEM images of individual MXene nanosheets deposited on a porous alumina plate. It can be seen that the MXene nanosheets are about 3-10 μm in

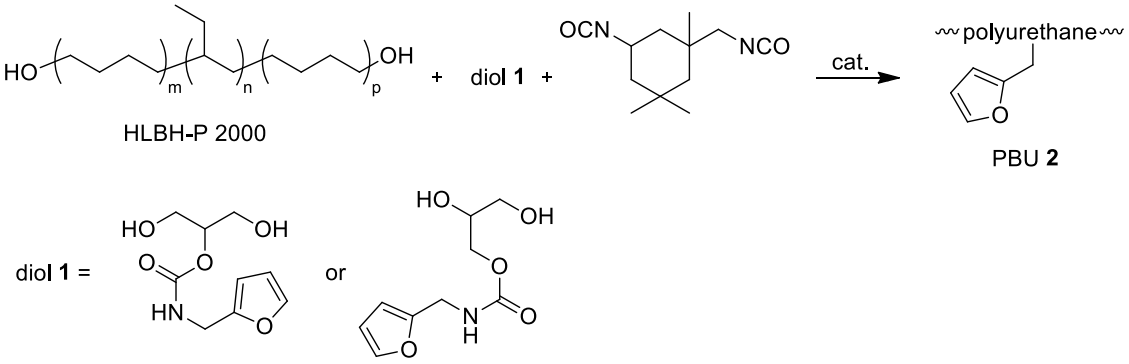

Scheme 1 Synthesis of PBU 2

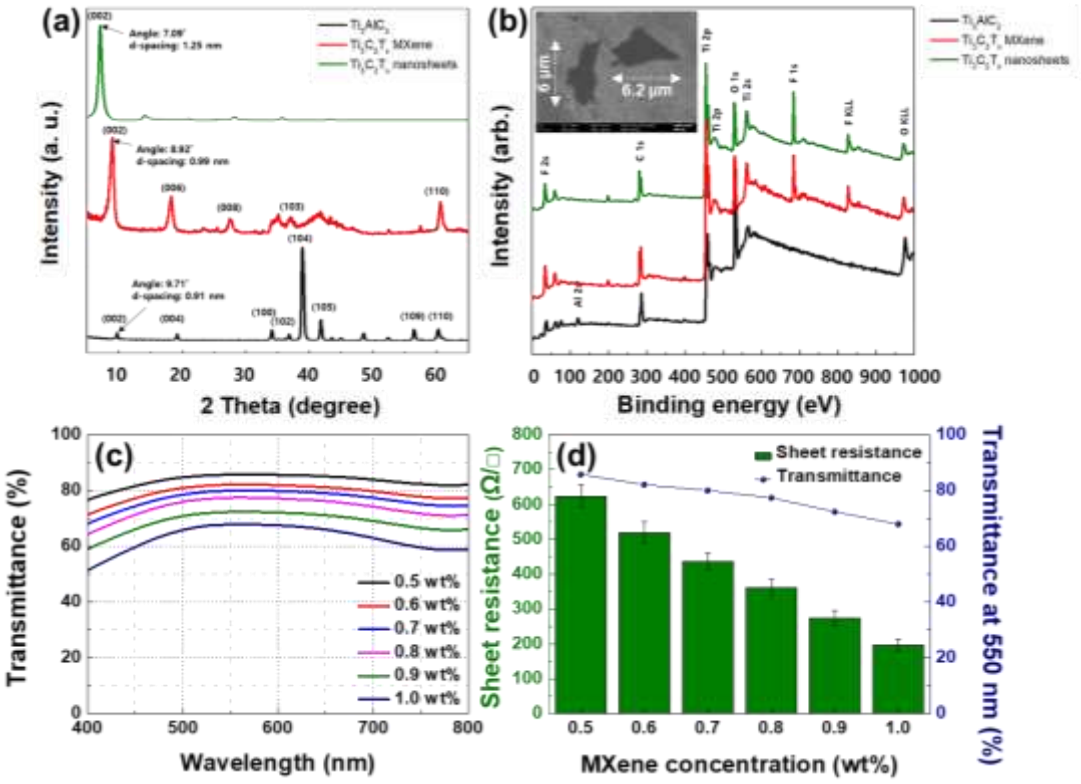

Fig. 3(a) XRD patterns and b XPS spectra of MAX (Ti_3AlC_2), multi-layered MXene (Ti_3C_2Tx), and monolayer MXene nanosheets (Ti_3C_2Tx). An inset FESEM micrograph in (b) shows monolayer MXene nanosheets on an alumina membrane filter. (c) Optical transmittance spectra of MXene nanosheets deposited on glass substrates. d Sheet resistance and optical transmittance (at 550 nm) of MXene nanosheets deposited on glass. Samples for the measurements were prepared by coating glass substrates with MXene nanosheet dispersions of various concentrations.

lateral dimension, and without agglomeration or stacking. In the XRD pattern of the individual MXene nanosheets shown in Fig. 3(a), the main peak is shifted to a lower angle (7.09°) than in the pattern of the MXene platelets. This corresponds to a d-spacing of 1.25 nm, which is higher than that of the MXene platelets, indicating that exfoliation has taken place (Tang *et al.* 2021). Fig. 3(b) shows the XPS survey spectra of the MAX powder, MXene platelets, and exfoliated MXene nanosheets. The major elements present in the Ti_3AlC_2 MAX powder are Ti, C, Al, and O. The XPS spectrum of the MXene platelets shows the absence of Al and the presence of F, which was likely introduced as a surface termination group. The XPS spectrum of individual MXene nanosheets shows the presence of Ti and C as the major elements, and smaller concentrations of O and F, probably as surface termination groups; this is consistent with the previously reported XPS results of individual MXene nanosheets with -F and -OH functional groups at the surfaces (Halim *et al.* 2016).

We also synthesized a new polymer, PBU 2, containing furan rings, for electrospinning (Scheme 1). The incorporation of the furan ring into the polyurethane backbone was achieved by employing diol 1 having a pendant furan ring (Pyo *et al.* 2016). The furan ring is

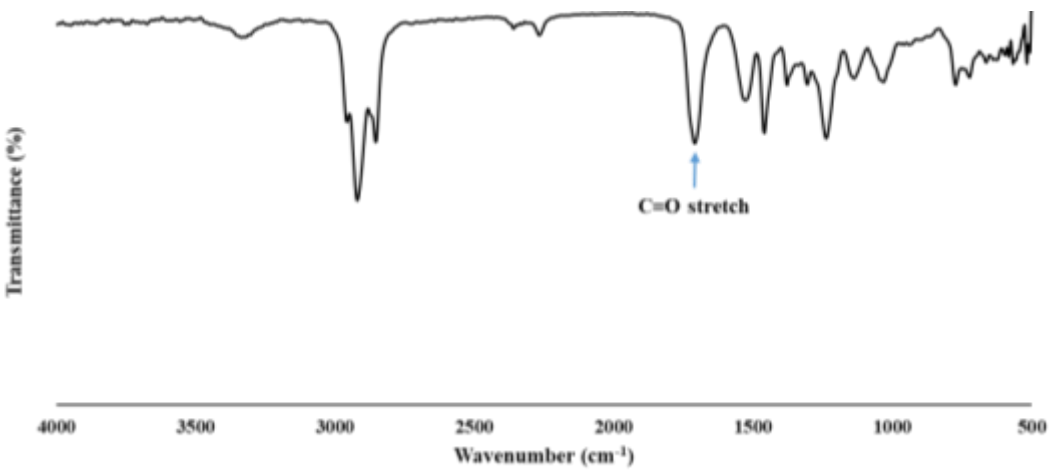

Fig. 4 FTIR spectrum of PBU 2

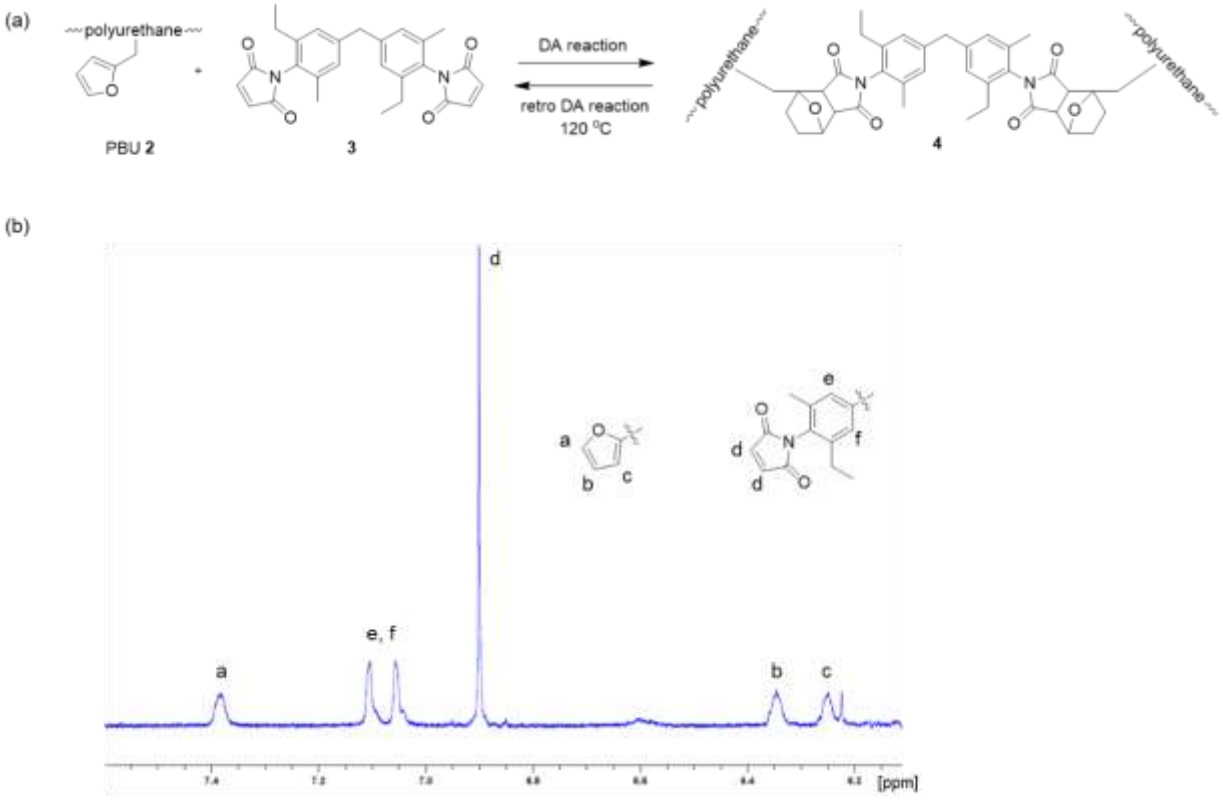

Fig. 5(a) DA and retro-DA reactions; (b) The 1H NMR spectrum of the compound 4 in C2D2Cl4 after heating at 120°C for 20 min. Due to the retro DA reaction the compound 4 was restored to PBU 2 and bismaleimide 3, which was indicated by the solubility of the products in $C_2D_2Cl_4$.

capable of reacting with maleimide to form a DA adduct at low temperatures (Oliveira *et al.* 2020) owing to its low activation energy (43 kJ/mol). The formation of DA adducts at relatively low temperatures allows crosslinking between the polymer microfibrils, thereby enhancing the mechanical stability of the porous film without disrupting their shape (Appuhamillage *et al.* 2017). In addition, PBU is suitable for fabricating stretchable pressure sensors as it exhibits elasticity and also allows a retro-DA reaction, which is critical to the self-healing property of the film. The reaction of polyol, diol 1, isocyanate and organotin catalyst in MEK facilitated the PBU 2 (Scheme 1). The viscosity of the PBU 2 solution with a solid content of *ca.* 50 wt.% was 1400 cps. The presence of the urethane bond in PBU 2 was confirmed by the characteristic absorbance peak at 1708 cm^{-1} in its FTIR spectrum (Fig. 4). The numeric average weight and average molecular weight of PBU 2 determined by GPC were 6,500 and 27,900 g/mol, respectively. The T_g of the PBU 2 determined by DSC analysis is approximately -48°C. Like other polymers with furan groups (Park *et al.* 2019, Heo *et al.* 2016), PBU 2 was cross-linked by bismaleimide 3 via a DA reaction to form product 4 (Fig. 5(a)), which was not soluble in organic solvents. To investigate the retro-DA reaction, the insoluble product 4 in

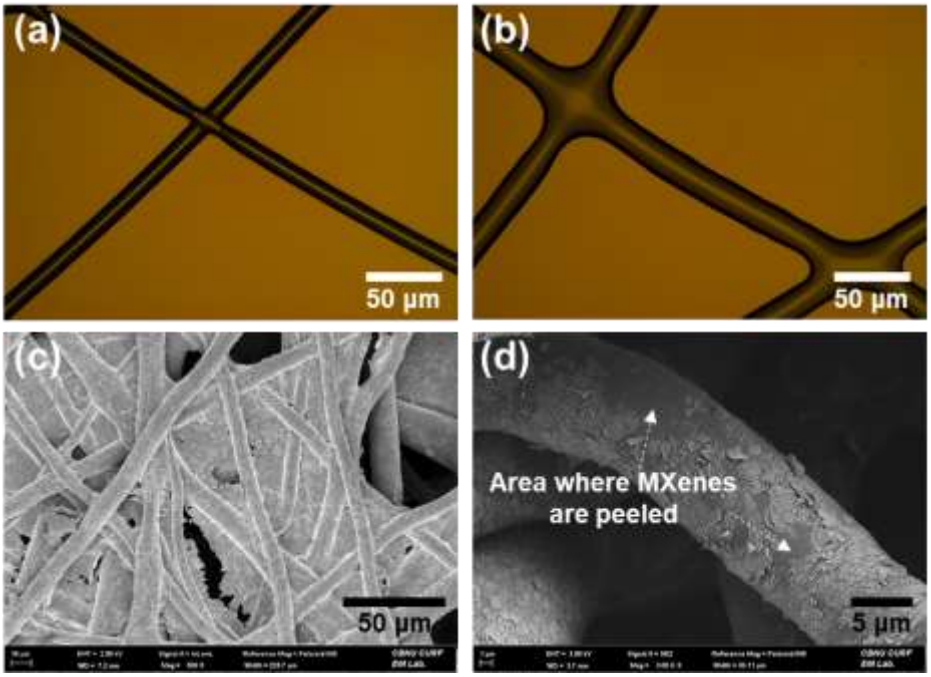

Fig. 6(a) As-electrospun microfibril network, and (b) microfibril network after DA reaction at 60°C for 3 h. Microfibrils in contact were covalently bonded to each other via the DA reaction. (c) Microfibril-based film surface with MXene nanosheets formed. (d) Microfibrils with MXene nanosheets after 10 min of ultrasonication. The MXene nanosheets were partially peeled off from the surface of the microfibrils.

$C_2D_2Cl_4$ was heated at 120°C for 20 min and the proton resonances were monitored by ^1H NMR spectroscopy (Fig. 5(b)). The proton peaks corresponding to the furan ring and maleimide appeared between 6.2 and 7.5 ppm, indicating the occurrence of the retro-DA reaction.

The porous film was fabricated by electrospinning on a layer of PDMS previously cast on a glass substrate to prevent the adhesion of the film to the glass surface. The average rate of increase in the thickness of the film is approximately 5.82 μm/min. We used this value to obtain films of desired thicknesses by adjusting the electrospinning time. The microfibrils-based network structure is key to realizing highly sensitive pressure sensors. It follows that the structure of the film should not be significantly altered by any subsequent processing. Nevertheless, it is important to note that the electrospun fibers are physically stacked against each other with no bonding between them, which can lead to friction between the fibers when the film is stretched. This can cause excessive shear stress at the interfaces of the fibers, which can ultimately lead to either slippage between the fibers or their deformation. This problem can be overcome by the formation of covalent bonds between the fibers at their interfaces. The activation energy for the formation of covalent bonds between PBU 2 chains via the DA reaction is low (43 kJ/mol). This enables crosslinking between the fibers at the relatively low temperature of 60°C. This low-temperature crosslinking process prevents deformation of the porous film by thermal expansion, melting, and fusion of the fibers. As shown in Fig. 6(a) and 6(b), after curing at 60°C for 3 h, integration between fibers is observed only in the regions where they are in contact with each other, while no significant changes in fiber shape occurred. The cured porous film was easily peeled from the PDMS layer, and it was used as a soft film for the pressure sensor.

Next, we made the porous film conducting by coating MXene nanosheets on the surfaces of the PBU fibers. This was achieved by dipping the film into a dispersion containing 0.8 wt% of MXene nanosheets. As shown in Fig. 6c, after only 1 min of dipping, a uniform coating of MXene nanosheets is formed on the surfaces of the fibers, likely owing to the abundance of hydroxyl termination groups on the surfaces of the MXene nanosheets. In addition, it should be noted that the layer of MXene nanosheets is contiguous, and it also covers the vacant regions between the fibers. However, the MXene nanosheets that are not bound to the fibers are likely to be separated from the film during repeated stretching/ relaxation cycles. Therefore, we removed these MXene burrs by sonicating the MXene-coated films for 10 min. FESEM image of the sonicated films shows that the treatment was effective in removing the MXene burrs (Fig. 6(d)). However, we observed that some MXene nanosheets were also detached from the fiber surface (Fig. 6(d)), which is probably owing to poor adhesion of the nanosheets to the fibers. Given that the MXene-coated porous film is likely to be subjected to repeated applications of pressure and stretching/relaxation cycles, the adhesion between these two materials is critical to the long-term reliability of the sensor.

Unlike flat surfaces, it is extremely difficult to achieve strong adhesion between nanomaterials and the peripheral and inner surfaces of polymer fibers forming a porous film. Reported techniques for attaching nanomaterials to flat films surfaces include the use of adhesives (Jiang *et al.*

2019), embedding (Abbas *et al.* 2018), and photo-induced heating (Kim *et al.* 2018). However, there are no reports of techniques for ensuring strong and uniform adhesion of nanomaterials to the surfaces of fibers meshed together to form a film. We resolved this issue by exploiting the reversible cross-linking capability of the PBU polymers. First, a porous film just coated with MXene nanosheets was heated at 120°C for 20 min to induce a retro-DA reaction causing the crosslinks formed earlier at the interfaces of the PBU fibers to reverse, ensuring surface flowability and stickiness. Unlike the melting of thermoplastic polymers, this heating process mainly affects the surfaces of the fibers without leading to the collapse of the fiber structures. Further, as the fiber surfaces are already completely covered by the MXene nanosheets, the fibers do not fuse together. The temporary increase in the polymer fluidity at the surfaces of the PBU fibers leads to increased wetting of the MXene nanosheets deposited on the fibers, and thereby ensures better adhesion between the nanosheets and the fibers. Thereafter, the film was heated at 60°C for 1 h to ensure the formation of crosslinks once again at the interfaces of the PBU fibers. The interface between the MXene and PBU fibers thus formed forms an exceptionally strong bond due to the large contact area and conformal contact between the two materials. By this procedure, we fabricated a porous, conducting PBU film with MXene nanosheets adhering securely to the PBU fiber surfaces for application as a sensor.

To evaluate the enhancement in adhesion between the MXene nanosheets and the PBU fibers by the retro-DA and subsequent DA reactions, we recorded the variation in the sheet resistance of the MXene-coated porous films with the time for which it was subjected to ultrasonication and with the number of tape test cycles. As shown in Fig. 7(a), for samples prior to the sequence of the retro-DA and DA reactions, the resistance of the porous film gradually increased with the duration of the ultrasonication treatment, and after about 60 min, it exceeded 1000% of its initial value. The resistance of the film subjected to the sequence of retro-DA and DA reactions initially showed a mild increase but did not change significantly thereafter. Given that the initial increase in resistance is likely owing to the removal of the MXene nanosheets burr, it is clear that subjecting the MXene-coated PBU film to the sequence of the retro-DA and DA reactions significantly improved the adhesion between MXene nanosheets and PBU fibers. As can be seen from the insets of Fig. 7(a), a significant amount of MXene nanosheets was removed from the fiber surface that was not subjected to the retro-DA and DA reactions after 60 min of ultrasonication, while MXene nanosheets were uniformly attached to the surface of the fiber that was subjected to this sequence of reactions. Similar trends were observed in the resistance measurements of the films subjected to repeated adhesive tape tests before and after the application of this sequence of reactions, as shown in Fig. 7(b). However, it can be seen that the resistance of samples increases to some extent even after the retro-DA and DA reactions. This may be because the PBU fibers are very soft, as a result of which the film undergoes significant deformation during tape delamination. Nevertheless, the difference in the trends in the two cases was evident, implying that the adhesion of MXene nanosheets to the PBU fibers was dramatically improved by the retro-DA and DA reactions.

We also evaluated the dynamic adhesion stability of the two materials through stretch-and-release cycling tests. As shown in Fig. 7(c), the difference between the resistance values before and after application of the uniaxial stretch continued to increase with repeated cycling before the retro-DA and DA reactions. In particular, maximum resistance under stretching increased from about 30 ohm to 10,000 ohm, while the increase rate remained almost constant until 1000 cycles. The samples that underwent the sequence of retro-DA and DA reactions showed a dramatic decrease in resistance increment, as shown in Fig. 7(d), and a decrease in the resistance increment rate with cycling. Scanning electron microscopy reveals significant differences between the surface of a PBU fiber that was not subjected to the retro-DA/DA reaction sequence, and that of a fiber that was subjected to this reaction sequence, after 1000 stretch-and-release cycles. While most of the MXene nanosheets were delaminated from the former (Fig. 7(e)), no significant detachment of MXene nanosheets can be seen for the latter (Fig. 7(f)). In Fig. 7(e), a surface crack is visible on the PBU fiber, whereas wrinkles can be seen on the surface of the fiber in Fig. 7(f). The wrinkles are likely the result of repeated tensile and compressive stresses generated by the stretch-and-release cycles in the MXene nanosheets, indicating excellent adhesion between the nanosheets and the PBU surface.

Next, we studied the self-healing properties of fabricated sensors. As shown in Fig. 8(a), an incision was made using a knife with a force of 0.3 N on the surface of a MXene-coated PBU porous film (Fig. 8(a-2)). After this the film was subjected to a retro-DA reaction at 120°C for 5 min and a DA reaction at 60 °C for 1 h (Fig. 8(a-3)). As shown in Fig. 8(a-3), the incision mark was removed without any changes in the morphology of the film. This remarkable self-healing behavior can be attributed to (1) the short time for retro-DA reaction, and (2) the surface fluidity caused by the retro-DA reaction, which enabled the re-establishment of contact and integration between the incised surfaces during the subsequent DA reaction. Fig. 8(b) shows that about half of the sensors were completely cut with scissors and then healed by the same process. As shown in Fig. 8(b-3), the incision did not reappear when the healed sample was subjected to uniaxial tensile stresses. In this case, the resistance and current changes of the sensors with cutting and healing were also measured, where the current was measured with the fixed voltage of 1 V (Fig. 8(c)). The increase in resistance as a result of the midway cut was mostly reversed after healing, and almost entirely reversed when the retro-DA reaction time was longer (10 min), allowing for complete healing. Current values showed a trend that was opposite to that of the resistance. Although a longer duration of the retro-DA reaction allows for more complete healing by increasing fluidity at the surfaces of the PBU fibers, excessively long retro-DA reaction times can cause the fibers to collapse. Thus, the retro-DA the PBU fibers, excessively long retro-DA reaction times can cause

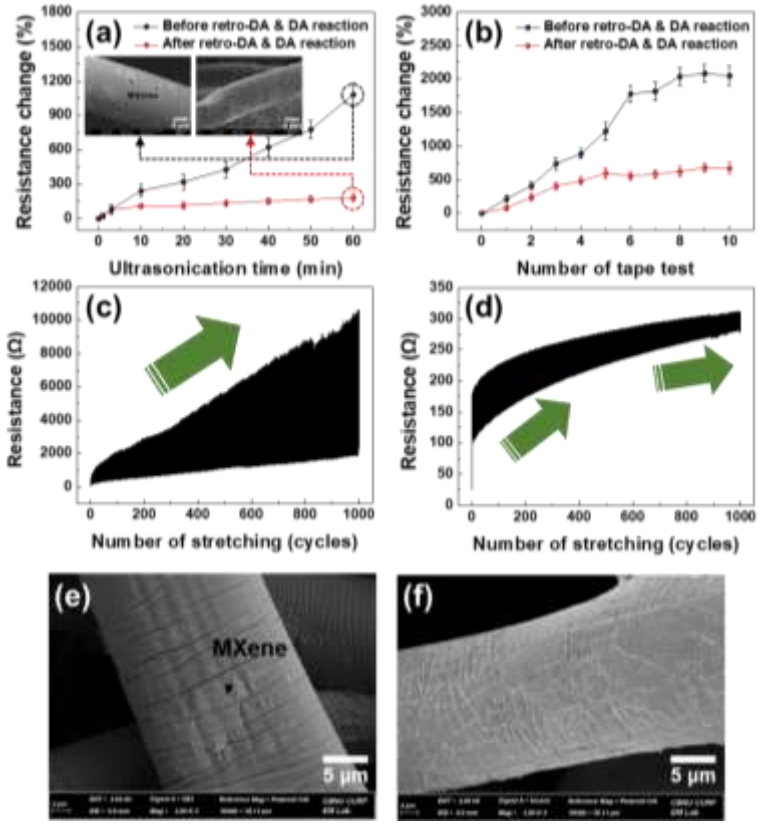

Fig. 7 Change in resistance of MXene nanosheets formed on PBU fiber network with (a) ultrasonication time and (b) number of adhesive tape delamination tests. In these tests, samples before and after retro-DA and DA reactions were used. Change in resistance of MXene nanosheets formed on PBU fiber network with number of stretching cycles (c) before and (d) after retro-DA and DA reactions. For stretch-and-release testing, a uniaxial strain of 50% was used. FESEM micrographs of PBU fiber surfaces with MXene nanosheets after 1000 cycles of stretch-and-release with 50% strain e before and f after retro-DA and DA reactions.

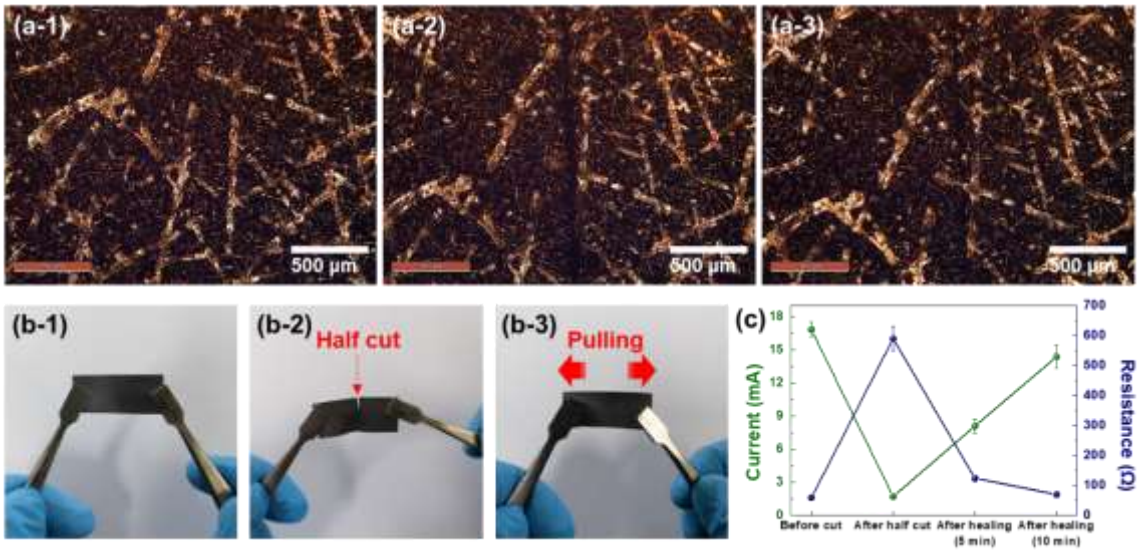

Fig. 8 Optical micrograph of porous film surface (a-1) before cutting, (a-2) after cutting mark formation, and (a-3) after a retro-DA reaction at 120°C for 5 min, and DA reaction at 60°C for 1 h. Changes in morphology were observed after healing. A sensor (b-1) before cutting, (b-2) after being cut down the middle, such that the dimension of the cut is equal to half its width, and (b-3) after a retro-DA reaction at 120°C for 5 min, and DA reaction at 60°C for 1 h. After healing, the sensor was pulled in the direction perpendicular to that of cutting. (c) Resistance and current changes of the sensors with cutting and healing, where the current was measured with the fixed voltage of 1 V. Healing time on the x-axis implies the retro-DA reaction time. The DA reaction condition was set equally at 60°C for 1 h.

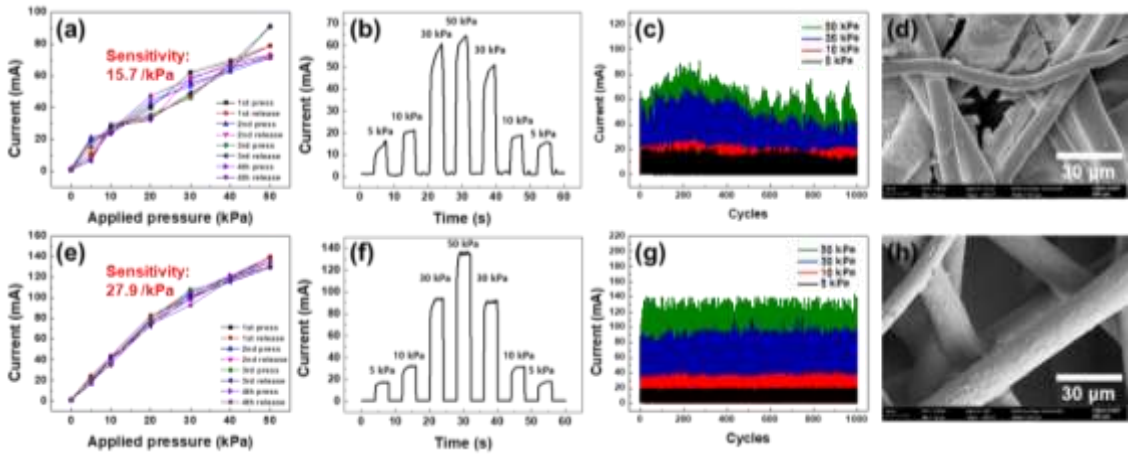

Fig. 9 Current measurements (a)-(d) for a sensor that has not been subjected to retro-DA and DA reactions, and (e)-(h) for a sensor that has been subjected to retro-DA reaction at 120°C for 20 min and DA reaction at 60°C for 1 h. Current measured with a and e repeated press-and-release cycles for up to 50 kPa, and (b) and (f) pressures of varying magnitude applied over time. (c) and (g) Current measured when various pressures are applied repeatedly for 1000 cycles. d and h FESEM micrographs of the sensor surface after 1000 cycles of application of a 50 kPa pressure followed by release.

the fibers to collapse. Thus, the retro-DA reaction should be carried out for only the requisite length of time to ensure healing. These results validate the self-healing behavior of the developed sensors.

Finally, we evaluated the pressure sensitivity of the sensors. The film with a thickness of 130 μm displayed high sensitivity at low applied pressures, but the sensitivity decreased with increasing pressure. Films with thicknesses of 320 and 380 μm displayed low overall sensitivity. The overall sensitivity has highest for the film with thickness 250 μm. Therefore, it was chosen as the optimum film thickness for further evaluation for sensor applications. The characteristics of a sensor which was not subjected to the retro-DA and DA reactions are shown in Figs. 9(a)-9(d), and those of a sensor that was subjected to the reactions are shown in Figs. 9(e)-9(h). Figs. 9(a) and 9(e) show the currents recorded after repeated application of various pressures on each sensor. In both cases, the films can be used to detect pressures up to approximately 50 kPa, but when higher pressures were applied, the changes in current with pressure were significantly reduced. This is owing to the rupturing of the conducting MXene nanosheet layer owing to excessive pressure. Overall, the sensor current increased with the applied pressure, which is likely owing to the decrease in the resistance in the MXene layer as a result of the formation of new contacts between the nanosheets under pressure. The sensitivity of the sensor that was not subjected to retro-DA and DA reactions was found to be 15.7 /kPa, and the current change behavior was somewhat unstable with repeated pressing and release. On the other hand, the sensor that was subjected to the reactions, shows a higher sensitivity of approximately 27.9 /kPa, and much better reproducibility of the currents. To the best of our knowledge, the sensitivity of 27.9 /kPa for 0 to 50 kPa is the highest one among the reported stretchable self-healing pressure sensors (Wang *et al.* 2018, Khan *et al.* 2020, Yang *et al.* 2021, Zhao *et al.* 2020, Robby *et al.* 2021).

Figs. 9(b) and 9(f) show the sensor currents when various pressures were applied in real time. For the sensor that has not been subjected to the retro-DA and DA reactions, the rise time is somewhat longer and the reproducibility is low (Fig. 9(b)), whereas for the sensor that has been stabilized by the reactions, both characteristics are improved (Fig. 9(f)). Figs. 9(c) and 9(g), which show the sensor currents with the repeated application of various pressures on the sensors for 1000 cycles, underscore the difference in the performance of the sensor that has not been subjected to the reactions and that which has been stabilized by the reactions. For the sensor that was not stabilized, the currents owing to the repeated application of pressure are not reproducible; however, for the sensor stabilized by the retro-DA and DA reactions, it is evident that the currents are much more reproducible. This improvement in the performance of the pressure sensor as a result of the retro-DA and DA reactions is owing to the significantly improved bonding stability between the MXene nanosheets and the PBU fibers. The currents through the MXene layer change as a result of variations in the contacts between the MXene nanosheets; when the MXene nanosheets are securely bonded to the PBU surfaces as a result of the retro-DA and DA reactions, the currents are reproducible even after multiple cycles of pressure application and relaxation, and the sensor exhibits reliable long-term performance. Figs. 9(d) and 9(h) show FESEM micrographs of the surfaces of the two sensors, following the application of a pressure of 50 kPa for 1000 cycles. Again, in the case of the sensor that was not subjected to the retro-DA and DA reactions, MXene nanosheets are significantly delaminated from the PBU fibers (Fig. 9(d)), while they are securely attached to the surfaces of the PBU fibers in the sensor that has been subjected to the reactions (Fig. 9(h)). These results show very clearly how the bonding between the two materials formed as a result of the retro-DA and DA reactions affects the performance of the sensor.

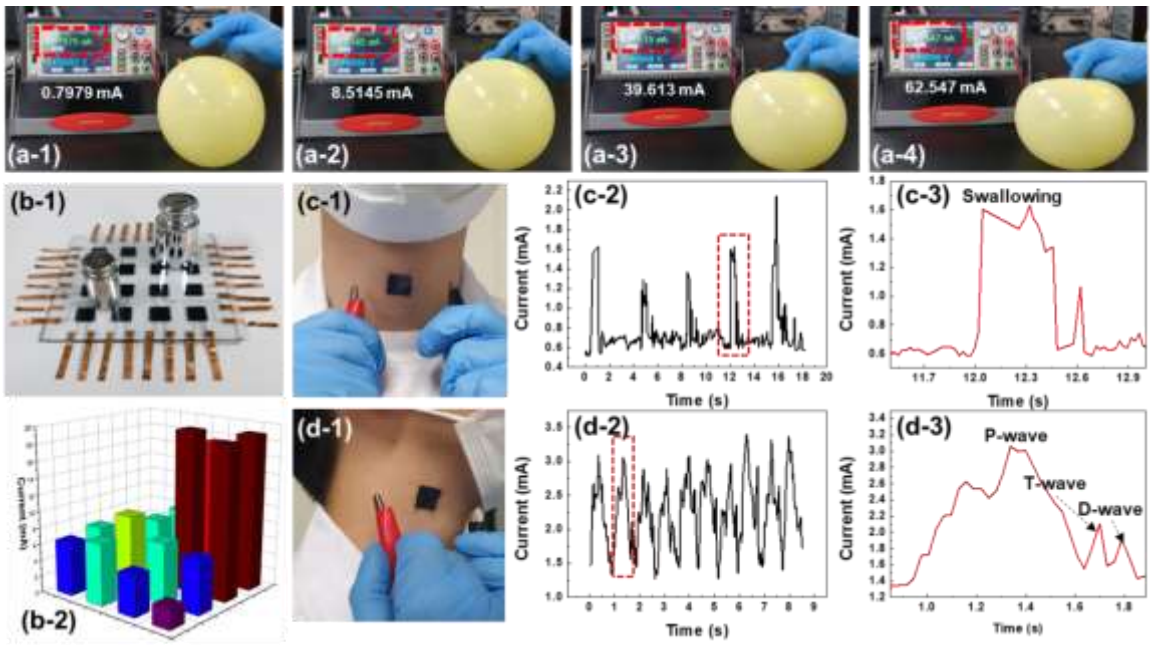

Fig. 10(a) Current measured whilst the tip of a gloved finger to which the sensor is attached is used to apply pressure to a balloon inflated with air. In each photograph, the red dotted square indicates the measured current, which is shown in white font below the square. (b-1) A sample of a 16-pixel sensor array with two weights on it. (b-2) Distribution chart for the currents measured at each pixel for the scenario depicted in (b-1). (c-1) A sensor attached to the front of a person's neck to detect the motion from swallowing. (c-2) Current measured from a sensor that was attached to the front of a person's neck to detect motion from swallowing. (c-3) Enlarged view of the portion indicated by the red dotted square in (c-1). (d-1) A sensor attached to the skin around the carotid artery to measure the wearer's pulse. (d-2) Current measured from a sensor attached to the skin around the carotid artery to measure the wearer's pulse. (d-3) Enlarged view of the portion indicated by the red dotted square in (d-1).

We evaluated the performance of our sensor in multiple ways as shown in Fig. 10. First, as shown in Fig. 10(a), the sensor was attached to the tip of a gloved finger, which was used to press a balloon injected with air, and the current response was recorded. As indicated by the red dotted square in the photographs, the recorded current increased in proportion to the pressure applied on the balloon. In order to apply the sensor in a multi-pixel pressure sensor array, a MXene nanosheet circuit was formed on a glass substrate. A total of 16 sensors were attached to the glass substrate on which the MXene circuit was formed (face-up), and another similar glass substrate with a MXene circuit was laminated on it (face-down) to implement a sandwich-structured sensor array. Fig. 10(b-1) shows a photograph of two different steel weights placed on the sensor array. The currents measured at each pixel are shown in Fig. 10(b-2). The value of the current measured precisely reflects the pressure distribution caused by the weights. The background current may be attributed to the distribution of the pressure exerted by the weights by the upper glass plate perpendicular to the direction of the weights. The pressure transmitted by the glass also affected the pixels far from the weights owing to the high sensitivity of the sensors.

Lastly, we fabricated a sensor for attachment to the human skin to track the physiological signals and activity. Here, in order to prevent MXene nanosheets from directly contacting the human body, two PBU films were used to cover the upper and lower surfaces of the sensor. The PBU in the sensor as well as in the outer layers was subjected to retro-DA and DA reactions to ensure mechanical integrity. The Cu wire for current measurement was connected to the sensor before the integration. This sensor was attached to the front of a person's neck using a commercial silicone-based adhesive (MG7-9850, Dow CORNING, USA) to detect the muscular motion resulting from swallowing (Fig. 10(c-1)). The measured current response (Figs. 10(c-2) and 10(c-3)) shows that the sensor was able to detect the motion of the sternal thyroid muscle when saliva passed through the esophagus. Further, we attached a sensor to the skin around the carotid artery to measure the wearer's pulse (Fig. 10(d-1)). Once again, the current response (Fig. 10(d-2)) showed that the sensor was able to detect the movement of the muscles as blood pumped through the carotid artery. In particular, the P-, T-, and D-waves could be clearly identified (Fig. 10(d-3)). Thus, we have demonstrated the suitability of our sensor for a range of applications, including those that require high sensitivity. To the best of our knowledge, there are no reports of pressure sensors in which stretchability, self-healing, high sensitivity, and high reliability have been realized simultaneously. This combination of characteristics in our sensors was enabled by the use of a PBU polymer that was capable of undergoing a DA reaction at a low temperature, porous network film enabled by electrospinning, and strong adhesion between high-quality MXene nanosheets and PBU fibers achieved by triggering retro-DA and DA reactions involving the PBU. Ensuring the uniform deposition and adherence of conductive nanomaterials on the peripheral

and inner surfaces of porous films is a prerequisite for implementing highly sensitive pressure sensors. However, we are unaware of any reports detailing approaches for accomplishing these objectives. The approach developed in this study is not limited by the morphology and structure of the materials involved, and can be used not only for MXene nanosheets, but also other types of conducting nanomaterials such as graphene and AgNWs. One weakness of this study is that the self-healing of the sensors still presupposes high temperatures (retro-DA and DA reaction), so it is difficult to implement while equipped on the human skin. This issue can be resolved if the temperatures for the reactions are further lowered, but in that case, the heat resistance of the devices it is directly related, so careful consideration is required.

4. Conclusions

This work was supported by a National Research Foundation of Korea (NRF) grant (Number 2018R1D1A1B 07047386 and 2020M3H4A3081895) funded by the Korean government (MSIP). Further support was provided by the Industry Technology R&D program (20006467 and 20006511) funded By the Ministry of Trade, Industry & Energy (MOTIE, Korea).

References

Abbas, S., Kumar, M., Kim, H.S., Kim, J., Lee, J.H. (2018), "Silver-nanowire-embedded transparent metal-oxide heterojunction Schottky photodetector", *ACS Appl. Mater. Interf*, **10**, 14292-14298. https://doi.org/10.1021/acsami.8b05141.

Alhabeb, M., Maleski, K., Anasori, B., Lelyukh, P., Clark, L., Sin, S., Gogotsi, Y. (2017), "Guidelines for synthesis and processing of two-dimensional titanium carbide ($Ti_3C_2T_x$ MXene)", *Chem. Mater.*, **29**, 7633-7644. https://doi.org/10.1021/acs.chemmater.7b02847.

Appuhamillage, G.A., Reagan, J.C., Khorsandi, S., Davidson, J. R., Voit, W., Smaldone, R.A. (2017), "3D printed remendable polylactic acid blends with uniform mechanical strength enabled by a dynamic Diels–Alder reaction", *Polym. Chem.*, **8**, 2087-2092. https://doi.org/10.1039/C7PY00310B.

Baby, T., Jose E.T., George, G., Varkey, V., Cherian, S.K. (2019), "A new approach for the shaping up of very fine and beadless UV light absorbing polycarbonate fibers by electrospinning", *Polym. Test.*, **80**, 106103. https://doi.org/10.1016/j.polymertesting.2019.106103.

Bai, N., Wang, L., Wang, Q., Deng, J., Wang, Y., Lu, P., Huang, J., Li, G., Zhang, Y., Yang, J., Xie, K., Zhao, X., Guo, C. F. (2020), "Graded intrafillable architecture-based iontronic pressure sensor with ultra-broad-range high sensitivity", *Nat. Commun.*, **11**, 209. https://doi.org/10.1038/s41467-019-14054-9.

Cai, G., Yu, Z., Tong, P., Tang, D. (2019), "Ti_3C_2 MXene quantum dot-encapsulated liposomes for photothermal immunoassays using a portable near-infrared imaging camera on a smartphone", *Nanoscale*, **11**, 15659-15667. https://doi.org/10.1039/C9NR05797H.

Chen, J., Li, Z., Ni, F., Ouyang, W., Fang, X. (2020), "Bio-inspired transparent MXene electrodes for flexible UV photodetectors", *Mater. Horizons*, **7**, 1828-1833. https://doi.org/10.1039/D0MH00394H.

Chen, J., Tong, P., Huang, L., Yu, Z., Tang, D. (2019), "Ti_3C_2 MXene nanosheet-based capacitance immunoassay with tyramine-enzyme repeats to detect prostate-specific antigen on interdigitated micro-comb electrode", *Electrochim. Acta*, **319**, 375-381. https://doi.org/10.1016/j.electacta.2019.07.010.

Cheng, B., Wu, P. (2021), "Scalable fabrication of Kevlar/ Ti_3C_2TxMXene intelligent wearable fabrics with multiple sensory capabilities", *ACS Nano*, **15**, 8676-8685. https://doi.org/10.1021/acsnano.1c00749.

Fu, X., Wang, L., Zhao, L., Yuan, Z., Zhang, Y., Wang, D., Wang, D., Li, J., Li, D., Shulga, V., Shen, G., Han, W. (2021), "Controlled assembly of MXene nanosheets as an electrode and active layer for high-performance electronic skin", *Adv. Funct. Mater.*, **31**, 2010533. https://doi.org/10.1002/adfm.202010533.

Halim, J., Cook, K.M., Naguib, M., Eklund, P., Gogotsi, Y., Rosen, J., Barsoum, M.W. (2016), "X-ray photoelectron spectroscopy of select multi-layered transition metal carbides (MXenes)", *Appl. Surf. Sci.*, **362**, 406-417. https://doi.org/10.1016/j.apsusc.2015.11.089.

Hantanasirisakul, K., Zhao, M.Q., Urbankowski, P., Halim, J., Anasori, B., Kota, S., Ren, C.E., Barsoum, M.W., Gogotsi, Y. (2016), "Fabrication of Ti_3C_2Tx MXene transparent thin films with tunable optoelectronic properties", *Adv. Electron. Mater.*, **2**(6), 1600050. https://doi.org/10.1002/aelm.201600050.

Heo, G., Pyo, K., Lee, D. H., Kim, Y., Kim, J.-W. (2016), "Critical role of Diels–Adler adducts to realise stretchable transparent electrodes based on silver nanowires and silicone elastomer", *Sci. Rep.*, **6**, 25358. https://doi.org/10.1038/srep25358 (2016).

Huang, C., Thomas, N.L. (2018), "Fabricating porous poly (lactic acid) fibres via electrospinning", *Eur. Polym. J.*, **99**, 464-476. https://doi.org/10.1016/j.eurpolymj.2017.12.025.

Huang, L., Yu, Z., Chen, J., Tang, D. (2020), "Pressure-based bioassay perceived by a flexible pressure sensor with synergistic enhancement of the photothermal effect", *ACS Appl. Bio Mater.*, **3**(12), 9156-9163. https://pubs.acs.org/doi/10.1021/acsabm.0c01447.

Jiang, Z., Nayeem, M.O.G., Fukuda, K., Ding, S., Jin, H., Yokota, T., Inoue, D., Hashizume, D., Someya, T. (2019), "Highly stretchable metallic nanowire networks reinforced by the underlying randomly distributed elastic polymer nanofibers via interfacial adhesion improvement", *Adv. Mater.*, **31**(37), 1903446. https://doi.org/10.1002/adma.201903446.

Kalani, S., Kohandani, R., Bagherzadeh, R. (2020), "Flexible electrospun PVDF-$BaTiO_3$ hybrid structure pressure sensor with enhanced efficiency", *RSC Adv.*, **10**(58), 35090. https://doi.org/10.1039/d0ra05675h.

Khan, A., Kisannagar, R.R., Gouda, C., Gupta, D., Lin, H.C. (2020), "Highly stretchable supramolecular conductive self-healable gels for injectable adhesive and flexible sensor applications", *J. Mater. Chem. A*, **8**(38), 19954-19964. https://doi.org/10.1039/D0TA07543D.

Kim, K.S., Choi, S. Bin, Kim, D.U., Lee, C.R., Kim, J.W. (2018), "Photo-induced healing of stretchable transparent electrodes based on thermoplastic polyurethane with embedded metallic nanowires", *J. Mater. Chem. A*, **6**(26), 12420-12429. https://doi.org/10.1039/C8TA02979B.

Lee, S., Franklin, S., Hassani, F.A., Yokota, T., Nayeem, M.O.G., Wang, Y., Leib, R., Cheng, G., Franklin, D.W., Someya, T. (2020a), "Nanomesh Pressure Sensor for Monitoring Finger Manipulation without Sensory Interference", *Science*, **370**, 966-970. https://doi.org/10.1126/science.abc9735.

Lee, Y., Kim, S.J., Kim, Y.J., Lim, Y., Chae, Y., Lee, B.J., Kim, Y.T., Han, H., Gogotsi, Y., Ahn, C.W. (2020b), "Oxidation-resistant titanium carbide MXene films", *J. Mater. Chem. A*, **8**(2), 573-581. https://doi.org/10.1039/C9TA07036B.

Li, J., Bao, R., Tao, J., Peng, Y., Pan, C. (2018), "Recent progress in flexible pressure sensor arrays: from design to applications", *J. Mater. Chem. C*, **6**(44), 11878-11892.

https://doi.org/10.1039/C8TC02946F.

Li, X., Chen, W., Qian, Q., Huang, H., Chen, Y., Wang, Z., Chen, Q., Yang, J., Li, J., Mai, Y.W. (2021), "Electrospinning-based strategies for battery materials", *Adv. Energy Mater.*, **11**(2), 2000845. https://doi.org/10.1002/aenm.202000845.

Liu, Q., Zhu, J., Zhang, L., Qiu, Y. (2018), "Recent Advances in Energy Materials by Electrospinning", *Renew. Sust. Energy Rev.*, **81**, 1825-1858. https://doi.org/10.1016/j.rser.2017.05.281.

Luo, J., Gao, S., Luo, H., Wang, L., Huang, X., Guo, Z., Lai, X., Lin, L., Li, R.K.Y., Gao, J. (2021), "Superhydrophobic and breathable smart MXene-based textile for multifunctional wearable sensing electronics", *Chem. Eng. J.*, **406**, 126898. https://doi.org/10.1016/j.cej.2020.126898.

Mannsfeld, S.C.B., Tee, B.C.K., Stoltenberg, R.M., Chen, C.V. H.H., Barman, S., Muir, B.V.O., Sokolov, A.N., Reese, C., Bao, Z. (2010), "Highly sensitive flexible pressure sensors with microstructured rubber dielectric layers", *Nat. Mater.*, **9**(10), 859-864. https://doi.org/10.1038/nmat2834.

Mehrez, S., Karati, S.A., DolatAbadi, P.T., Shah, S.N.R., Azam, S., Khorami, M., Asslizadeh, H. (2020), "Nonlocal dynamic modeling of mass sensors consisting of graphene sheets based on strain gradient theory", *Adv. Nano Res.*, **9**(4), 221-235. http://doi.org/10.12989/anr.2020.9.4.221.

Moraveji, M., Keshvari, H., Karkhaneh, A., Bonakdar, S., Hadi, A., Haghighipour, N. (2021), "The effect of collagen/ polycaprolactone fibrous scaffold decorated with graphene nanoplatelet and low-frequency electromagnetic field on neuronal gene expression by stem cells", *Adv. Nano Res.*, **10**(6), 549-557. http://doi.org/10.12989/anr.2021.10.6.549.

Oliveira, J.C., Laborie, M.P., Roucoules, V. (2020), "Thermodynamic and kinetic study of Diels–Alder reaction between furfuryl alcohol and N-Hydroxymaleimides—An assessment for materials application", *Molecules*, **25**(2), 243. https://doi.org/10.3390/molecules25020243.

Park, K.H., Shin, C., Song, Y.S., Lee, H.J., Shin, C., Kim, Y. (2019), "Recyclable and mendable cellulose-reinforced composites crosslinked with Diels–Alder adducts", *Polymers*, **11**(1), 117. https://doi.org/10.3390/polym11010117.

Pyo, K., Lee, D. H., Kim, Y., Kim, J. (2016), "Extremely rapid and simple healing of a transparent conductor based on Ag nanowires and polyurethane with a Diels–Alder network", *J. Mater. Chem. C*, **4**(5), 972-977. https://doi.org/10.1039/C5TC04030B.

Robby, A.I., Lee, G., Lee, K.D., Jang, Y.C., Park, S.Y. (2021), "GSH-responsive self-healable conductive hydrogel of highly sensitive strain-pressure sensor for cancer cell detection", *Nano Today*, **39**, 101178. https://doi.org/10.1016/j.nantod.2021.101178.

Ruth, S.R.A., Feig, V.R., Tran, H., Bao, Z. (2020), "Microengineering Pressure Sensor Active Layers for Improved Performance", *Adv. Funct. Mater.*, **30**(39), 2003491. https://doi.org/10.1002/adfm.202003491.

Sang, Z., Ke, K., Manas-Zloczower, I. (2019), "Design strategy for porous composites aimed at pressure sensor application", *Small*, **15**(45), 1903487. https://doi.org/10.1002/smll.201903487.

Seok, S.H., Choo, S., Kwak, J., Ju, H., Han, J.H., Kang, W.S., Lee, J., Kim, S.Y., Lee, D.H., Lee, J., Wang, J., Song, S., Jo, W., Jung, B.M., Chae, H.G., Son, J.S., Kwon, S.Y. (2021), "Synthesis of high quality 2D carbide MXene flakes using a highly purified MAX precursor for ink applications", *Nanosc. Adv.*, **3**(2), 517-527. https://doi.org/10.1039/D0NA00398K.

Shi, J., Wang, L., Dai, Z., Zhao, L., Du, M., Li, H., Fang, Y. (2018), "Multiscale hierarchical design of a flexible piezoresistive pressure sensor with high sensitivity and wide linearity range", *Small*, **14**(27), 1800819. https://doi.org/10.1002/smll.201800819.

Tang, J., Huang, X., Qiu, T., Peng, X., Wu, T., Wang, L., Luo, B., Wang, L. (2021), "Interlayer Space Engineering of MXenes for Electrochemical Energy Storage Applications", *Chem. A Eur. J.*, **27**(6), 1921-1940. https://doi.org/10.1002/chem.202002283.

Thirumoorthi, M., Thomas Joseph Prakash, J. (2016), "Structure, optical and electrical properties of indium tin oxide ultra thin films prepared by jet nebulizer spray pyrolysis technique", *J. Asian Ceram. Soc.*, **4**(1), 124-132. https://doi.org/10.1016/j.jascer.2016.01.001.

Xiao, J., Tan, Y., Song, Y., Zheng, Q. (2018), "A flyweight and superelastic graphene aerogel as a high-capacity adsorbent and highly sensitive pressure sensor", *J. Mater. Chem. A*, **6**(19), 9074-9080. https://doi.org/10.1039/C7TA11348J.

Xiong, Y., Shen, Y., Tian, L., Hu, Y., Zhu, P., Sun, R., Wong, C. P. (2020), "A flexible, ultra-highly sensitive and stable capacitive pressure sensor with convex microarrays for motion and health monitoring", *Nano Energy*, **70**, 104436. https://doi.org/10.1016/j.nanoen.2019.104436.

Wang, T., Zhang, Y., Liu, Q., Cheng, W., Wang, X., Pan, L., Xu, B., Xu, H. (2018), "A self-healable, highly stretchable, and solution processable conductive polymer composite for ultrasensitive strain and pressure sensing", *Adv. Funct. Mater.*, **28**(7), 170551. https://doi.org/10.1002/adfm.201705551.

Wang, W., Zheng, Y., Jin, X., Sun, Y., Lu, B., Wang, H., Fang, J., Shao, H., Lin, T. (2019), "Unexpectedly high piezoelectricity of electrospun polyacrylonitrile nanofiber membranes", *Nano Energy*, **56**, 588-594. https://doi.org/10.1016/j.nanoen.2018.11.082.

Wang, Y., Chao, M., Wan, P., Zhang, L. (2020), "A wearable breathable pressure sensor from metal-organic framework derived nanocomposites for highly sensitive broad-range healthcare monitoring", *Nano Energy*, **70**, 104560. https://doi.org/10.1016/j.nanoen.2018.11.082.

Yang, J.C., Kim, J.O., Oh, J., Kwon, S.Y., Sim, J.Y., Kim, D.W., Choi, H.B., Park, S. (2019), "Microstructured porous pyramid-based ultrahigh sensitive pressure sensor insensitive to strain and temperature", *ACS Appl. Mater. Interfaces*, **11**(21), 19472-19480. https://doi.org/10.1021/acsami.9b03261.

Yang, Z., Li, H., Zhang, S., Lai, X., Zeng, X. (2021), "Superhydrophobic MXene@ carboxylated carbon nanotubes/ carboxymethyl chitosan aerogel for piezoresistive pressure sensor", *Chem. Eng. J.*, **425**, 130462. https://doi.org/10.1016/j.cej.2021.130462.

Yu, X., Yu, X., Zhang, J., Chen, L., Long, Y., Zhang, D. (2017), "Optical properties of conductive silver-nanowire films with different nanowire lengths", *Nano Res.*, **10**(11), 3706-3714. https://doi.org/10.1007/s12274-017-1583-6.

Yu, Z., Cai, G., Tong, P., Tang, D. (2019), "Saw-toothed microstructure-based flexible pressure sensor as the signal readout for point-of-care immunoassay", *ACS Sens.*, **4**(9), 2272-2276. https://pubs.acs.org/doi/10.1021/acssensors.9b01168.

Yu, Z., Cai, G., Liu, X., Tang, D. (2020), "Platinum nanozyme-triggered pressure-based immunoassay using a three-dimensional polypyrrole foam-based flexible pressure sensor", *ACS Appl. Mater. Interf.*, **12**(36), 40133-40140. https://pubs.acs.org/doi/10.1021/acsami.0c12074.

Zeng, R., Tao, J., Tang, D., Knopp, D., Shu, J., Cao, X. (2020), "Biometric-based tactile chemomechanical transduction: An adaptable strategy for portable bioassay", *Nano Energy*, **71**, 104580. https://doi.org/10.1016/j.nanoen.2020.104580.

Zeng, R., Wang, W., Chen, M., Wan, Q., Wang, C., Knopp, D, Tang, D. (2021), "CRISPR-Cas12a-driven MXene-PEDOT:PSS piezoresistive wireless biosensor", *Nano Energy*, **82**, 105711. https://doi.org/10.1016/j.nanoen.2020.105711.

Zhang, C., Nicolosi, V. (2019), "Graphene and MXene-based transparent conductive electrodes and supercapacitors", *Energy Storage Mater.*, **16**, 102-125. https://doi.org/10.1016/j.ensm.2018.05.003.

Zhao, W., Qu, X., Xu, Q., Lu, Y., Yuan, W., Wang, W., Wang, Q., Huang, W., Dong, X. (2020), "Ultrastretchable, self-healable, and wearable epidermal sensors based on ultralong Ag nanowires composited binary-networked hydrogels", *Adv. Electron. Mater.*, **6**(7), 2000267. https://doi.org/10.1002/aelm.202000267.

Zholobko, O., Wu, X.F., Zhou, Z., Aulich, T., Thakare, J., Hurley, J. (2020), "A comparative experimental study of the hygroscopic and mechanical behaviors of electrospun nanofiber membranes and solution-cast films of polybenzimidazole", *J. Appl. Polym. Sci.*, **137**(39), e49639. https://doi.org/10.1002/app.49639.

Zhu, Z., Li, R., Pan, T. (2018), "Imperceptible epidermal–iontronic interface for wearable sensing", *Adv. Mater.*, **30**(6), 1705122. https://doi.org/10.1002/adma.201705122.

Zhu, Y., Wu, Y., Wang, G., Wang, Z., Tan, Q., Zhao, L., Wu, D. (2020), "A flexible capacitive pressure sensor based on an electrospun polyimide nanofiber membrane", *Org. Electron.*, **84**, 105759. https://doi.org/10.1016/j.orgel.2020.105759.